Individual Nanotube-Based Needle Nanoprobes for Electrochemical Studies in Picoliter Microenvironments

Kyungsuk Yum, Han Na Cho, Jie Hu, and Min-Feng Yu*

Department of Mechanical Science and Engineering, University of Illinois at Urbana–Champaign, 1206 West Green Street, Urbana, Illinois 61801

ABSTRACT We report the fabrication and characterization of individual nanotube-based, long and straight needle nanoprobes for electrochemistry and the study of their applicability and behavior in microenvironments. The needle nanoprobe, with a nanoscale ring-shaped Au electrode at the tip of the needle serving as the active electrode, was characterized by electrochemical current measurement and cyclic voltammetry and analyzed with electrochemical models. Such a needle nanoprobe, in combination with another metal-coated nanowire as a reference electrode, was further used, for the first time, for local electrochemical sensing inside microdroplets having volumes down to a few picoliters. We explain the acquired voltammetric behaviors of redox-active molecules in confined microscale environments and reveal a unique electrochemical mechanism which allows the regeneration of the redox-active molecules and the establishment of a stable reference potential in the microenvironments.

KEYWORDS: nanotube nanoprobe · electrochemical sensing · cyclic voltammetry · microenvironment

Nanoscale electrode probes capable of probing microenvironments provide exciting new opportunities for fundamental and applied studies in nanoscale science and technology. In the context of electrochemistry, the small dimensions of the electrode probes increase the temporal and spatial resolutions as well as enhance mass transport rate at the electrodes. Such characteristics have allowed the study of fast heterogeneous electron transfer kinetics,[1] detection of single molecules,[2] electrochemical analysis in small volumes,[3–5] and investigation of the local electrochemical activity of heterogeneous surfaces (*e.g.*, *via* scanning electrochemical microscopy).[6] In addition, the small electrode probes with microscale and nanoscale dimensions have enabled novel biological applications,[7] such as intracellular biomolecular sensing,[8–10] measuring neurophysiological signals,[11,12] and real-time monitoring of cell exocytosis.[13,14] Although several techniques have been developed in fabricating nanoprobes having electroactive areas with characteristic dimensions down to a few nanometers at the apex, these existing nanoelectrode probes have a tapered shape and, correspondingly, a relatively large total structure, except for the very end of the probe,[15–24] limiting their range of applicability for nonintrusive electrochemical studies in isolated microenvironments.[25–28]

Due to their well-defined nanoscale geometry and excellent mechanical, electrical, and chemical properties, nanotubes have recently been explored as electrodes for electrochemistry, overcoming the aforementioned problems in nanoelectrode fabrication. Campbell *et al.*[29] reported the direct use of individual multiwall carbon nanotubes having diameters of ~150 nm for electrochemistry. Heller *et al.*[30] demonstrated the use of individual single-wall carbon nanotubes laid on substrate surface as nanoelectrodes for electrochemistry. Burt *et al.*[31] presented the development of electrochemically insulated carbon nanotube-based probes with overall probe diameters of ~400 nm for combined scanning electrochemical microscopy and atomic force microscopy. However, none of these reported studies has fully exploited one of the most unique features of nanotubes as a nanoscale electrochemical probe—the high length-to-diameter aspect ratio—or demonstrated their electrochemical sensing capabilities in microenvironments. For instance, high aspect ratio nanoneedles (200–300 nm in diameter)[32] and nanotubes[33–36] have only recently been used as biological probes for intracellular studies with minimal invasiveness, such as surgery and manipulation of single living cells[32] and precise delivery of molecules into cells without

*Address correspondence to mfyu@uiuc.edu.

Received for review August 15, 2007 and accepted November 20, 2007.

Published online December 08, 2007
10.1021/nn700171x CCC: $37.00

damaging them.[33–36] However, for the extended use of such nanoscale electrode probes for electrochemical applications in microenvironments, including those within living cells, an understanding of the behavior of nanoelectrodes in microenvironments should first be developed, which has thus far been lacking.

In this article, we report the fabrication and characterization of individual nanotube-based needle nanoprobes for electrochemical studies and the study of their electrochemical applicability and behavior in microenvironments. To our knowledge, our nanotube-based electrochemical nanoprobes have the smallest total structural diameter (including coating layers), ~100 nm, among needle-shaped nanoprobes having uniform diameter along their length (over more than 10 μm), in addition to having well-defined nanoscale geometries with the high aspect ratio optimized for probing microenvironments. Each nanotube nanoprobe typically has an electrochemically active area of ~1000 nm^2, and the characteristic dimension of the nanoelectrodes can be precisely controlled in our fabrication process. The nanotube nanoprobes were thoroughly characterized by electrochemical current measurement and cyclic voltammetry to determine their functionality. The voltammetric responses of the nanotube nanoprobes were found to fit the classical Butler–Volmer model well. We further demonstrate the applicability and the voltammetric behavior of such high aspect ratio nanotube nanoprobes in microdroplets having volumes down to a few picoliters, and we reveal a novel electrochemical mechanism in confined microenvironments where the redox-active molecules can be regenerated and dominate the electrochemical reaction at the reference electrode, establishing a stable reference potential. Further development could well extend the use of such nanoprobes to microenvironments with dimensions down to a few micrometers or a volume of ~1 fL[37] and to electrochemical studies at the single-molecule level in microenvironments (*e.g.*, *via* redox cycling).[2,38] In addition, taking advantage of the hollow structure of the nanotubes with excellent mechanical properties, the nanotube nanoprobes could be further exploited for manipulation,[32] delivery of molecules,[33–36] and spatially resolved electrical and electrochemical measurements inside microenvironments.

RESULTS AND DISCUSSION

Fabrication of Nanotube Nanoprobes. The nanotube nanoprobe was fabricated by first attaching a semiconducting boron nitride nanotube (BNNT)[39–41] onto a metal microelectrode probe, then coating the attached BNNT consecutively with thin conformal layers of metal and insulating polymer, and finally cutting off the very end of the coated BNNT. This process yielded a coaxial cable-like probe with a ring-shaped nanoelectrode exposed at the very end of the probe. The total structural

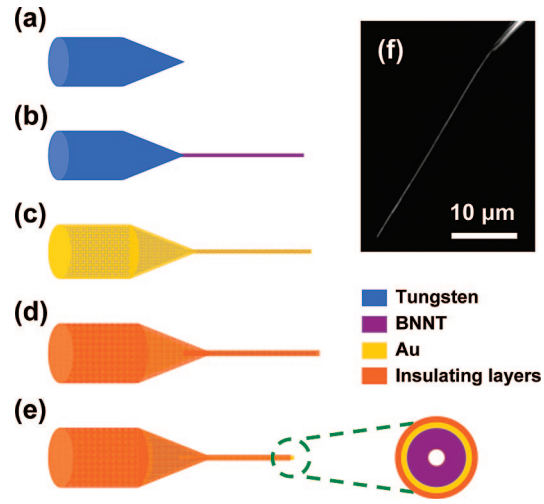

Figure 1. Schematic showing the consecutive steps in the nanoprobe fabrication process: (a) a sharpened metal wire, (b) the attachment of a nanotube onto the metal wire, (c) sputter-coating of Au, (d) electropolymerization coating of insulating polymer layers, and (e) focused ion beam cutting of the nanoprobe end and the zoomed view of the cross-sectional structure of the probe end. (f) Optical microscope image of a fabricated nanotube electrochemical probe.

diameter of the fabricated nanotube nanoprobe was ~100 nm, including the metal and insulating layers, and the length was ~10−30 μm.

Figure 1a−e illustrates the fabrication process. Individual BNNTs with diameters from 30 to 100 nm and lengths from 10 to 40 μm were selected and used for the fabrication. A selected BNNT was attached to the tip of an electrochemically sharpened tungsten wire (Figure 1a) that would serve as a macroscopic handle for the easy use of the nanotube nanoprobe (Figure 1b).[42] The attached BNNT was sputter-coated with a thin layer (10−30 nm in thickness) of Au, Ag, or Pt to form an electrically conductive layer (Figure 1c). To increase the uniformity of the metal coating, the BNNT was sputter-coated twice on opposite sides. The thickness of the metal layer was accurately determined by measuring the diameter of the BNNT before and after the coating in a high-resolution scanning electron microscope (SEM) (XL30 ESEM, Philips). The nanotube was thoroughly rinsed with ethanol before and after the metal coating.

The metal-coated BNNT was then insulated with a thin conformal polymer layer by electropolymerization (Figure 1d). Polyphenol was chosen as the insulating layer because it is continuous, highly insulating, and free of pinhole defects. In addition, because the electropolymerization process is self-limiting, a very thin conformal insulation coating of typically ~10 nm in thickness can be realized.[43,44] This coating method differs from previously reported ones in that the electropolymerization of polyphenol in this method was performed in a strongly acidic solution[29,43] and that a protective silane layer was used to further improve the stability of the polyphenol layer.[44] The electropolymer-

ization initiated in a strongly acidic solution provides a thinner, less permeable polyphenol layer than that prepared in a less acidic solution.[29] Silane is cross-linked on polyphenol and significantly enhances the stability of the polyphenol layer.[44]

After the electrical insulation, the electrochemically active area was revealed by cutting off the end of the coated BNNT to a desired length by using a focused ion beam (FIB) (Dual-Beam DB-235, FEI, Inc.), which exposed a ring-shaped nanoelectrode (Figure 1e). During the cutting process, the exposure of the coated BNNT to electron or ion beams was minimized, and the coated BNNT was imaged only at low magnification to prevent any damage to the insulating layer. Typically, the coated BNNT was imaged first in the FIB microscope with the use of a very small ion beam current of ~1 pA to get the coordinates of the BNNT and then cut by scanning the ion beam with a current of 500 pA on a selected line across the BNNT for 5−10 s, depending on the diameter of the BNNT. After the FIB cutting, the exposed ring electrode at the extreme end of the BNNT became bright and could be identified in SEM at times.

The advantage in the use of a BNNT over a carbon nanotube for the nanoprobe fabrication is that, because a BNNT is a semiconductor with a wide band gap, the electrochemically active area is solely defined by the thickness of the metal coating and can thus be controlled precisely. Besides, a BNNT has excellent mechanical properties, similar to those of a carbon nanotube.[40,41] Au and Ag were primarily used as the coating materials in this study and served as the working and reference nanoelectrode materials, respectively. In principle, any conductive materials compatible with the sputter-coating process[31,45] or the electrochemical deposition process[46] can be used as electrode materials. Reference nanoprobes for electrochemical studies were prepared by sputter-coating Ag on Au-coated nanotubes without a further coating of the insulating layer.

Characterization of Nanotube Nanoprobes in Bulk Solutions. We first tested the electrical insulation of the nanotube nanoprobes by electrochemical current measurement in bulk solutions. An electric potential, sufficient for a redox reaction, was applied to the nanotube nanoprobe, and the current was monitored as the nanoprobe was moved in and out of a solution containing an electroactive species using a piezo-driven nanopositioning stage (P-752, PI). Figure 2 shows two typical electrochemical current profiles as the nanotube nanoprobe passes through the air/oil/aqueous solution interfaces of two sample solutions: 1.2 mM $Fc(CH_2OH)_2$ and 2.0 mM $Ru(NH_3)_6^{3+}$. When the nanoprobe entered the solution, the current rose sharply and reached a steady-state value. The steady-state current was maintained at a constant value as long as the nanoelectrode was immersed in the solution. When the nanoprobe was withdrawn from the solution, the current was sustained beyond the original solution/oil interface due to the meniscus formation between the nanoprobe and the aqueous solution. The meniscus was elongated at the solution/oil interface during the withdrawal process until broken, and at that instant, the current dropped to zero. The current responses in Figure 2 confirmed that the side wall of the nanotube nanoprobe was well insulated against both oxidation and reduction in the aqueous solution, and only the exposed end of the nanoprobe was active in the electrochemical process. For comparison, for an uninsulated Au-coated nanotube having a diameter of ~100 nm, the current varied linearly with immersion depth with a slope of ~0.4 nA/μm. The nanotube nanoprobes also showed good insulation in aqueous solutions in the presence or absence of a supporting electrolyte, *e.g.*, the reduction of $Ru(NH_3)_6^{3+}$ in the presence and in the absence of a KCl supporting electrolyte, and in organic solvents, *e.g.*, the oxidation of ferrocene in 1-octanol containing tetrabutylammonium tetrafluoroborate as a supporting electrolyte (data not shown here).

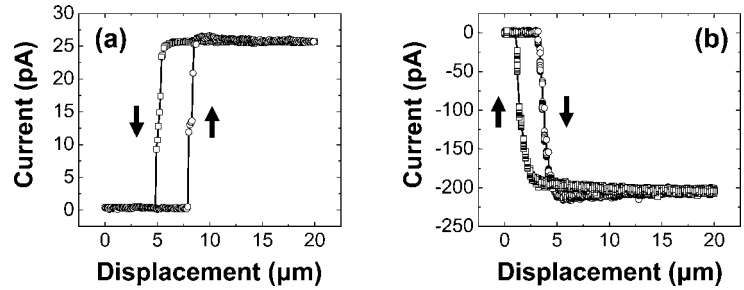

Figure 2. Electrochemical current measurement at the air/oil/aqueous solution interfaces of (a) a nanoelectrode (80 nm Au-coated nanotube with 10 nm Au layer) at the applied potential of 350 mV (*vs* Ag wire) in 1.2 mM $Fc(CH_2OH)_2$ in 25 mM KCl and (b) a nanoelectrode (140 nm Au-coated nanotube with 15 nm Au layer) at the applied potential of −500 mV (*vs* Ag/AgCl wire) in 2.0 mM $Ru(NH_3)_6^{3+}$ in 20 mM KCl. The nanoelectrodes were moved into (○) and withdrawn from (□) the aqueous solutions at the speed of 1 μm/s.

Figure 3 shows the typical voltammetric responses of the nanotube nanoprobes in bulk solutions. The voltammetric curves in panels a and b of Figure 3 correspond to the oxidation of $Fc(CH_2OH)_2$ and the reduc-

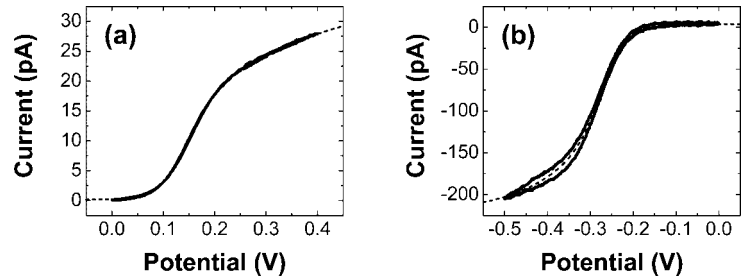

Figure 3. Cyclic voltammograms of (a) a nanoelectrode with diameter of 80 nm in a solution containing 1.2 mM $Fc(CH_2OH)_2$ and 25 mM KCl at a scan rate of 10 mV/s (potential *vs* Ag wire quasi-reference electrode (QRE)) and (b) a nanoelectrode with a diameter of 140 nm in a solution containing 2.0 mM $Ru(NH_3)_6^{3+}$ in 20 mM KCl at a scan rate of 100 mV/s (potential *vs* Ag/AgCl wire QRE). The dashed lines indicate the fits of eq 1 to the experimental data (solid lines).

tion of $Ru(NH_3)_6^{3+}$, respectively, in the presence of a KCl supporting electrolyte. The observed sigmoidal shape of the current–voltage responses is the characteristic steady-state behavior of a well-behaved small electrode, indicating again the good performance of the nanotube nanoprobes. The voltammetric curves were found to deviate from the Nernstian behavior and display the typical behavior of quasi-reversible electrode reactions. This deviation was attributed to the enhanced rate of mass transport at the nanoelectrodes, as described below. The voltammetric responses of the nanoprobes were stable during the time period of our experiments, at least for several hours. However, at times, a decrease in the current response was observed, due to the contamination of the active electrode area in the solution.

The steady-state voltammetric responses of the nanotube nanoprobes can be described by the Butler–Volmer model, combining the heterogeneous electrode kinetics with the diffusive mass transport:[47,48]

$$i = \frac{i_d}{1 + e^{\mp F(E-E'_0)/RT} + K_0^{-1} e^{\mp F\beta(E-E'_0)/RT}} \quad (1)$$

where i_d is the diffusion-limited current, F is the Faraday constant, R is the molar gas constant, T is the absolute temperature, E is the applied potential, E'_0 is the formal potential of the redox couple, and K_0 is the dimensionless heterogeneous rate constant, $K_0 = FAC^*k^O/i_d$, where A is the area of the electrode surface, C^* is the bulk concentration of the electroactive species, and k^O is the standard heterogeneous rate constant. In eq 1, the negative sign and $\beta = 1 - \alpha$ are used for oxidation, and the positive sign and $\beta = \alpha$ are used for reduction, where α is the transfer coefficient. The diffusivities of the reduced and oxidized species are assumed to be the same. The dashed lines in Figure 3 are fits of eq 1 to the experimental voltammograms (solid lines), where i_d, E'_0, α, and K_0 are used as fitting parameters, and $F/RT = 38.92\ V^{-1}$. Equation 1 describes the experimental voltammetric curves very well, yielding $i_d = 33.2 \pm 0.2$ pA, $E'_0 = 157.5 \pm 0.3$ mV, $\alpha = 0.838 \pm 0.003$, and $K_0 = 1.10 \pm 0.01$ for $Fc(CH_2OH)_2$ (Figure 3a) and $i_d = -225.7 \pm 1.6$ pA, $E'_0 = -278.9 \pm 0.4$ mV, $\alpha = 0.230 \pm 0.008$, and $K_0 = 1.44 \pm 0.01$ for $Ru(NH_3)_6^{3+}$ (Figure 3b). These values are not very sensitive to the values of α. For example, $K_0 = 1.05 \pm 0.01$ is obtained by fixing $\alpha = 0.7$ for $Fc(CH_2OH)_2$.

The diffusion-limited current of a ring-shaped nanoelectrode with thin insulation around its circumference can be approximated by considering a hemispherical-shaped electrode on an insulating plane having the same diameter as the outer diameter of the ring-shaped nanoelectrode:[25]

$$i_d = \pi FDC^* d_o \quad (2)$$

where D is the diffusion coefficient and d_o is the outer diameter of the nanoelectrode. It is recognized that if the radius of the insulation plane enclosing the electrode is less than twice the radius of the electrode, the diffusion from the half-space behind the plane needs to be included, which can increase the diffusion-limited current.[4,19,25,49,50] Simply modeling the thinly insulated electrode in our nanoprobe as a ring-shaped electrode on an insulated full plane underestimates the diffusion-limited current. A hemispherical-shaped electrode on an insulation plane approximates the nanoelectrode in our nanoprobe better when an analytical solution for the diffusion-limited current is desired in the analysis.[4,25] Taking $D = 6.4 \times 10^{-6}$ for $Fc(CH_2OH)_2$,[51] $D = 8.9 \times 10^{-6}$ cm^2/s for $Ru(NH_3)_6^{3+}$,[52] and the corresponding values of the diffusion-limited current i_d obtained previously, the outer diameters of the nanoelectrodes used in the measurements for parts a and b of Figure 3 are then calculated to be 140 and 420 nm, respectively. These calculated diameters are larger than the designed diameters of the nanoelectrodes measured in SEM, which are 80 and 140 nm, respectively. This discrepancy can arise from two possible causes. One is the enhanced diffusion for the nanotube nanoprobe from behind the nanoelectrode plane. The nanotube nanoprobe has a slender shape as compared to the conventional conical-shaped probes, which facilitates the broadened diffusion from the back of the nanoelectrode plane. The other is the nonideal FIB cutting, which may accidentally expose the side wall of the metal-coated nanotube near the tip of the nanoprobe. Certainly, questions remain whether the classical continuum description of mass transport is adequate to describe the voltammetric behavior at the nanoelectrode.[18,53–55] The larger discrepancy between the calculated and designed diameters observed for charged $Ru(NH_3)_6^{3+}$ ions than for neutral $Fc(CH_2OH)_2$ ions may also be related to the nonlinear ion transport behavior at the nanoelectrodes.[55] Due to the nanoscale dimension of the thickness of the ring-shaped electrode (~10 nm) in the nanotube nanoprobe and the expected high current density at this electrode, nonequilibrium conditions can be induced in the electrical double layer by the high ionic flux of charged species,[55] which is not considered in the derivation of eq 2. Nevertheless, until an advanced model for nanoelectrode is available, eq 2 is useful in providing an estimate of the apparent electroactive area of such nanoelectrodes.[4,18]

The cyclic voltammetry also allows us to access the kinetic information of the electrode reaction. The mass transport rate at the nanoelectrode is expected to be enhanced significantly due to the nanoscale dimensions of both the overall structure of the nanotube nanoprobe and the electroactive electrode area and the high current density at the ring-shaped electrode. The rate of mass transport can thus become comparable to

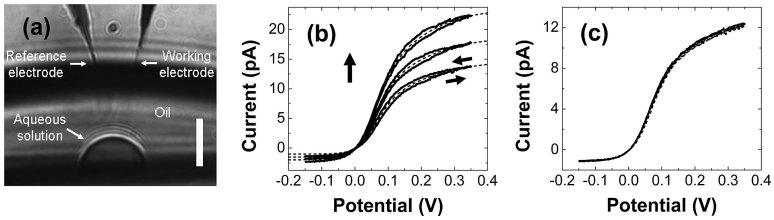

Figure 4. Electrochemistry of nanotube nanoprobes in microdroplets of aqueous solutions. (a) Optical microscope image of the electrochemical experiment in a microdroplet of an aqueous solution inside an oil droplet. The scale bar is 10 μm. (b) Cyclic voltammetric responses of three consecutive cycles of a nanotube nanoprobe in a microdroplet of an aqueous solution with a volume of ~2 pL, containing $Fc(CH_2OH)_2$ as an electroactive species and KCl as a supporting electrolyte, at a scan rate of 5 mV/s (potential *vs* nanowire reference electrode). The dashed lines are the fitting curves. (c) Cyclic voltammograms of three full forward and backward scans obtained from the reconstruction of the cyclic voltammetric curves in panel b after compensating for the increase of the solution concentration.

or greater than the rate of heterogeneous electron transfer. The acquired voltammetric response with the nanoelectrode thus includes the contributions to the electrochemical reaction of both the mass transport and the electrode kinetics and so deviates from the Nerstian behavior. The contribution of the kinetics of the electrode reaction in the cyclic voltammogram is explicitly included as $K_0^{-1}\, e^{\mp F\beta(E-E'_0)/RT}$ in eq 1, where $K_0^{-1} \approx 1$ from our modeling described above. Applying eq 2 and considering $A = \pi d_{app}^2/2$ for the equivalent hemispherical-shaped electrode, the standard heterogeneous rate constant is given by $k^0 = 2DK_0/d_{app}$. Based on the values of K_0 obtained from the fits in Figure 3, $k^0 = 1.0$ cm/s with $\alpha = 0.84$ for $Fc(CH_2OH)_2$ and $k^0 = 0.6$ cm/s with $\alpha = 0.23$ for $Ru(NH_3)_6^{3+}$. These values are in good agreement with literature values, for example, $k^0 = 0.4$ cm/s with a fixed $\alpha = 0.5$ for $Fc(CH_2OH)_2$ at spherical Au electrodes having diameters of 150 and 300 nm,[20] and $k^0 = 0.6$ cm/s and $\alpha = 0.3$ for $Ru(NH_3)_6^{3+}$ at a Pt electrode having a diameter of 25 μm.[52] We obtain $k^0 = 0.45$ cm/s with a fixed $\alpha = 0.5$ for $Fc(CH_2OH)_2$.

Electrochemistry in Microenvironments. A unique advantage of the developed nanotube nanoprobe is its use for electrochemical sensing in microenvironments. To demonstrate this applicability, we prepared a sample system consisting of a hemispherical aqueous microdroplet of femto- to picoliter in volume (5−20 μm in radius) inside a water-saturated mineral-oil layer (10−30 μm in height) on a silicon substrate. Figure 4a shows an optical microscope image of a typical electrochemical experiment in the microdroplet. The microdroplet was formed using micropipets mounted on a nanomanipulator equipped with a microinjection pump under an optical microscope.[37] Once the droplet was made, both working and quasi-reference/counter nanoprobes were maneuvered into the microscale aqueous droplet with the nanomanipulator. Electrochemical measurements were performed following the same procedure for the bulk solutions described above.

The nanotube nanoprobe penetrated the oil layer and reached the water droplet without causing any visible disturbance to the water droplet or the oil layer or forming any noticeable meniscus at the interfaces (Figure 4a). This would be difficult for conventional, conical-shaped microelectrodes with relatively large total structures. Here, the function of the oil layer was two-fold. First, the oil layer served as a protecting layer to prevent evaporation of the aqueous solution to attain stable electrochemical measurements. Second, the microdroplet consisting of two immiscible liquids was employed as a model system that mimics a living cell, a potential target for the unique application of such high aspect ratio nanotube nanoprobes.

Figure 4b shows typical voltammetric responses of a nanotube nanoprobe with a ring-shaped nanoelectrode in an aqueous microdroplet with a volume of ~2 pL, where an Ag-coated nanowire was used as a quasi-reference/counter electrode and $Fc(CH_2OH)_2$ and KCl were used as the electroactive species and the supporting electrolyte, respectively. The voltammograms in the figure show three cycles acquired sequentially. The well-defined sigmoidal shape of the voltammetric curves indicates a good performance of the nanoelectrode and stability of the nanowire reference electrode in the microenvironment. The appearance of sigmoidal curves implies also that the nanoelectrode remains small enough relative to the environment that the radial diffusion dominates the activity of the nanoelectrode in this configuration. The cyclic voltammograms in Figure 4b display a quasi-steady-state behavior and show that the current increases continuously during the measurement. This continuous increase in current is due to the increase of the concentration of the electroactive species, resulting from the evaporation of water in the droplet. Although the water droplet was covered with a water-saturated oil layer, evaporation of water was observed in the time scale of the experiment. The hysteresis observed between the forward and backward scans in each cycle, where the current of the backward scan is larger than that of the forward one, was again attributed to the increase in the concentration of the solution according to the further analysis described below. The small negative current observed on the negative side of potential corresponds to the reduction of the oxidized $Fc(CH_2OH)_2^+$ ions.

To quantify the obtained cyclic voltammograms in the microdroplet, we analyzed the measured voltammetric curves with the current-overpotential equation derived from the Butler–Volmer model:[56]

$$i_m = i_0 \frac{e^{(1-\alpha)\eta F/RT} - e^{-\alpha\eta F/RT}}{1 + \frac{i_0}{i_{d,a}} e^{(1-\alpha)\eta F/RT} - \frac{i_0}{i_{d,c}} e^{-\alpha\eta F/RT}} \quad (3)$$

where i_m is the measured current, i_0 is the exchange current, $\eta = E - E_{eq}$ is the overpotential, where E_{eq} is the equilibrium potential, and $i_{d,a}$ and $i_{d,c}$ are the anodic and cathodic limiting currents, respectively. The dashed lines in Figure 4b are the fittings of eq 3 to the experimental curves. Fittings were applied to the average values of the forward and backward scans in each cycle. The average values from the fittings of the three cycles in Figure 4b are $i_0 = 12.7 \pm 2.4$ pA, $\alpha = 0.78 \pm 0.01$, and $E_{eq} = 2.8 \pm 0.1$ mV. The total limiting currents, $i_{d,a} - i_{d,c}$, for the three cycles were also obtained from the curve fittings and are 16, 20, and 26 pA for the first, second, and third cycles, respectively. The average concentration of the total redox species in each cycle was then estimated according to eq 2 and was calculated to be 1.6, 2.0, and 2.5 mM during the first, second, and third scans in Figure 4b, respectively.[57] However, caution should be exercised when interpreting the obtained results, because the macroscopic relations of the nanoelectrodes may not be valid in microenvironments.[3–5] For instance, the diameter of the nanoelectrode (~50 nm) estimated according to the measured current in the microdroplet was smaller than the designed diameter (~80 nm).[57] Due to the restricted space in the microdroplet, the diffusion pattern around the working electrode was believed to be different from that in the bulk environment, which could lead to a deficit in the supply of the electroactive species at the working electrode.[4,5,58] The macroscopic relations (eq 2) may thus underestimate the concentration of the microdroplet.[5]

We reconstructed the cyclic voltammograms in the microdroplet (shown in Figure 4b) by compensating for the increase in the concentration of the solution according to $i_c = i_m C_i / C(t)$, where i_c is the compensated current, C_i is the initial concentration of the solution, and $C(t)$ is the concentration of the solution at time t. $C(t)$ was determined by fitting a second-order polynomial function to the concentrations (1.6, 2.0, and 2.5 mM) estimated previously for each cycle in Figure 4b. The time interval between the cycles is 200 s. The fitted polynomial is $C(t) = C_i(1 + 0.0013t + 6 \times 10^{-7}t^2)$.[59] Figure 4c shows the concentration-compensated replots of the three cycles in Figure 4b. The excellent overlap of the concentration-compensated voltammetric curves confirms that the hysteresis observed in Figure 4b was the result of the increase in the solution concentration during the measurement. The compensated voltammetric curves obtained from the microdroplet in Figure 4c are very similar to those from the bulk solution (Figure 3a) except for a negative shift in potential (the equilibrium potential is established at zero). This shift is attributed to a unique electrochemical mechanism in microscale electrochemical environments, as discussed below.

In a microscale electrochemical environment (*e.g.*, in a microdroplet), due to the confinement of both reduced/oxidized molecules and the close proximity of the working and reference electrodes, new electrochemical activities impossible in a bulk solution can be initiated. In our experiments, we observed a stable equilibrium potential of $E_{eq} = 0$ (*versus* the nanowire reference electrode) and a fixed concentration ratio of $Fc(CH_2OH)_2$ to $Fc(CH_2OH)_2^+$ ($C_R^*/C_O^* = 12.5 \pm 0.5$) in the three sequential cycles of the voltammograms acquired from a concentration-varying microenvironment (Figure 4b,c). This led us to conclude that, in the microenvironment, as the redox-active molecules were oxidized and reduced in either the working or the reference electrode, both the oxidized and reduced molecules became sufficiently available for both the working and reference electrodes and subsequently dominated the electrochemical reaction process, resulting in the fixed composition of the redox-active molecules and the stable reference potential as further explained below.

First, according to the equilibrium potential (open-circuit potential) given by the Nernst equation,[56,60]

$$E_{eq} = E^{0'} + \frac{RT}{F} \ln \frac{C_O^*}{C_R^*} \quad (4)$$

where C_O^* and C_R^* are the concentrations of the oxidized and reduced molecules in the microdroplet, respectively, a zero equilibrium potential can be attained only when the same redox reactions in the reverse directions occur separately at the working and reference electrodes, and a steady state with a fixed composition of the redox-active molecules (*e.g.*, $C_R^*/C_O^* = 12.5 \pm 0.5$ in Figure 4c) was reached. We have then $E_{eq,w} = E_{eq,r}$, where $E_{eq,w}$ and $E_{eq,r}$ (*versus* a standard reference electrode) are the equilibrium potentials of the working and reference electrodes respectively, and $E_{eq} = E_{eq,w} - E_{eq,r} = 0$, where E_{eq} is the equilibrium potential *versus* the nanowire reference electrode.

Second, a simple estimate indicates that the microdroplet with a volume of 2 pL and a concentration of 2.5 mM contains only 5 fmol of the electroactive $Fc(CH_2OH)_2$ molecules. However, the net number of molecules converted from $Fc(CH_2OH)_2$ to $Fc(CH_2OH)_2^+$, given by $F^{-1}\int i\,dt$, is calculated to be 12, 17, and 21 fmol according to the first, second, and third cycles in Figure 4b, respectively, much more than the available molecules in the original solution. This implies that, while the redox-active $Fc(CH_2OH)_2$ molecules were being oxidized at the working electrode, they were being continuously reproduced at the reference electrode and available for the working electrode (due to the small

volume of the microdroplet and the proximity between the electrodes), and *vise versa*. Otherwise, the small amount of available molecules in the microdroplet would be quickly consumed, and a fixed composition of the reduced and oxidized molecules observed in our measurement would never be established.

Such an electrochemical mechanism is practically not possible for nanoprobes used in a bulk environment. In a bulk environment, the small amount of oxidized molecules produced at the nanoprobes can hardly result in any appreciable concentration change that can alter the general electrochemical process or be significant enough to lead to the observation of a cathodic current as shown in Figure 4b in our microenvironment measurement; neither can the reduced molecules or ions from the reference probe be immediately available for the working electrode. The existence of such a unique mechanism of electrochemical electrodes in microenvironments can potentially simplify the development and application of nanoelectrode probes for standardized and quantitative studies in microenvironments.

CONCLUSION

The development of a novel nanotube-based high aspect ratio electrochemical probe was described, and the fabrication and characterization of the probe were detailed. Nanotube nanoprobes with well-defined electrode geometry and controllable diameters and lengths were fabricated. A reliable insulation procedure was implemented to obtain the well-insulated side walls of the nanotube nanoprobes. Stable voltammetric responses were acquired using such nanotube nanoprobes with ring-shaped nanoelectrodes and were described well with the classical Butler–Volmer model. The demonstration and study of the applicability and behavior of such nanoprobes in microenvironments further revealed a unique electrochemical mechanism in microscale electrochemical environments through cyclic voltammetry studies. The studies showed that the redox-active molecules could be regenerated and could be available to both the working and reference electrodes, which subsequently dominated the electrochemical reaction at the reference electrode and established a stable and self-adjusting reference potential. Such nanoscale, high aspect ratio nanotube nanoprobes could thus become unique tools for electrochemical and electrical studies in microenvironments, *e.g.*, single living cells or single synapses of neurons, with high spatial resolution and minimal disturbance of the environment and could potentially impact a broad spectrum of fundamental and applied studies in nanoscale science and technology.

EXPERIMENTAL METHODS

Insulation of Nanotube Nanoprobes. The nanotube nanoprobes were insulated with a thin conformal polymer layer by electropolymerization. The polyphenol layer was deposited by applying a cyclic potential between 0.0 and 0.8 V (*vs* Ag wire) onto the metal-coated BNNT in a highly acidic phenol solution (50 mM phenol in 0.5 M H_2SO_4) for 60 min. The polyphenol-coated BNNT was rinsed in water. The same process was repeated one day after the first electropolymerization. After the second electropolymerization coating of polyphenol, a silane layer was deposited on the polyphenol layer by cycling the deposition potential between 0.0 and 0.6 V in a 5 mM (3-aminopropyl)trimethoxysilane (3-ATS) solution for a few minutes. The fully coated BNNT was then rinsed in water and dried in air overnight. The phenol and 3-ATS solutions were prepared daily.

Electrochemical Measurements. The nanotube nanoprobes were characterized by electrochemical current measurement and cyclic voltammetry. Ferrocenedimethanol ($Fc(CH_2OH)_2$, Aldrich) and $Ru(NH_3)_6^{3+}$ (Strem) were used as electroactive species and KCl (Aldrich) as a supporting electrolyte. All aqueous solutions were prepared with 18 MΩ · cm water from a Milli-Q purification system (Millipore). Electrochemical responses were measured with home-built LabVIEW programs (National Instruments) using a patch clamp amplifier (EPC 7, HEKA) in a two-electrode configuration. Ag and Ag/AgCl wires were employed as the reference/counter electrodes for $Fc(CH_2OH)_2$ and $Ru(NH_3)_6^{3+}$, respectively. To prevent solution evaporation, the aqueous solutions were covered with a thin layer of mineral oil (~5 μm in thickness).

Acknowledgment. We thank Prof. A. Gewirth for helpful discussions. We appreciate Y. Bando and C. Tang of National Institute for Materials Science in Japan for providing us with the BN nanotube material. The work is supported by the National Science Foundation under Awards No. DMI 0328162 and No. CBET 0731096. The microscopy analyses involved in this work were carried out in the Center for Microanalysis of Materials at the University of Illinois, which is partially supported by the U.S. Department of Energy under grant DEFG02-91-ER45439.

REFERENCES AND NOTES

1 Penner, R. M.; Heben, M. J.; Longin, T. L.; Lewis, N. S. Fabrication and Use of Nanometer-Sized Electrodes in Electrochemistry. *Science* **1990**, *250*, 1118–1121.
2 Fan, F. R. F.; Bard, A. J. Electrochemical Detection of Single Molecules. *Science* **1995**, *267*, 871–874.
3 Clark, R. A.; Hietpas, P. B.; Ewing, A. G. Electrochemical Analysis in Picoliter Microvials. *Anal. Chem.* **1997**, *69*, 259–263.
4 Clark, R. A.; Ewing, A. G. Characterization of Electrochemical Responses in Picoliter Volumes. *Anal. Chem.* **1998**, *70*, 1119–1125.
5 Kashyap, R.; Gratzl, M. Electrochemistry in Microscopic Domains. 1. The Electrochemical Cell and Its Voltammetric and Amperometric Response. *Anal. Chem.* **1998**, *70*, 1468–1476.
6 *Scanning Electrochemical Microscopy*; Bard, A. J., Mirkin, M. V., Eds.; Marcel Dekker: New York, 2001.
7 Wightman, R. M. Probing Cellular Chemistry in Biological Systems with Microelectrodes. *Science* **2006**, *311*, 1570–1574.
8 Meulemans, A.; Poulain, B.; Baux, G.; Tauc, L.; Henzel, D. Micro Carbon Electrode for Intracellular Voltammetry. *Anal. Chem.* **1986**, *58*, 2088–2091.
9 Chien, J. B.; Wallingford, R. A.; Ewing, A. G. Estimation of Free Dopamine in the Cytoplasm of the Giant Dopamine Cell of Planorbis Corneus by Voltammetry and Capillary Electrophoresis. *J. Neurochem.* **1990**, *54*, 633–638.
10 Abe, T.; Lau, Y. Y.; Ewing, A. G. Intracellular Analysis with an Immobilized-Enzyme Glucose Electrode Having a 2-

μm Diameter and Subsecond Response Times. *J. Am. Chem. Soc.* **1991**, *113*, 7421–7423.
11 Phillips, P. E. M.; Stuber, G. D.; Heien, M. L. A. V.; Wightman, R. M.; Carelli, R. M. Subsecond Dopamine Release Promotes Cocaine Seeking. *Nature (London)* **2003**, *422*, 614–618.
12 Qiao, Y.; Chen, J.; Guo, X.; Cantrell, D.; Ruoff, R.; Troy, J. Fabrication of Nanoelectrodes for Neurophysiology: Cathodic Electrophoretic Paint Insulation and Focused Ion Beam Milling. *Nanotechnology* **2005**, *16*, 1598–1602.
13 Wightman, R. M.; Jankowski, J. A.; Kennedy, R. T.; Kawagoe, K. T.; Schroeder, T. J.; Leszczyszyn, D. J.; Near, J. A.; Diliberto, E. J., Jr.; Viveros, O. H. Temporally Resolved Catecholamine Spikes Correspond to Single Vesicle Release from Individual Chromaffin Cells. *Proc. Natl. Acad. Sci. U.S.A.* **1991**, *88*, 10754–10758.
14 Wu, W. Z.; Huang, W. H.; Wang, W.; Wang, Z. L.; Cheng, J. K.; Xu, T.; Zhang, R. Y.; Chen, Y.; Liu, J. Monitoring Dopamine Release from Single Living Vesicles with Nanoelectrodes. *J. Am. Chem. Soc.* **2005**, *127*, 8914–8915.
15 Shao, Y.; Mirkin, M. V.; Fish, G.; Kokotov, S.; Palanker, D.; Lewis, A. Nanometer-Sized Electrochemical Sensors. *Anal. Chem.* **1997**, *69*, 1627–1634.
16 Katemann, B. B.; Schuhmann, W. Fabrication and Characterization of Needle-Type Pt-Disk Nanoelectrodes. *Electroanalysis* **2002**, *14*, 22–28.
17 Slevin, C. J.; Gray, N. J.; Macpherson, J. V.; Webb, M. A.; Unwin, P. R. Fabrication and Characterisation of Nanometre-Sized Platinum Electrodes for Voltammetric Analysis and Imaging. *Electrochem. Commun.* **1999**, *1*, 282–288.
18 Conyers, J. L.; White, H. S. Electrochemical Characterization of Electrodes with Submicrometer Dimensions. *Anal. Chem.* **2000**, *72*, 4441–4446.
19 Watkins, J. J.; Chen, J.; White, H. S.; Abruna, H. D.; Maisonhaute, E.; Amatore, C. Zeptomole Voltammetric Detection and Electron-Transfer Rate Measurements Using Platinum Electrodes of Nanometer Dimensions. *Anal. Chem.* **2003**, *75*, 3962–3971.
20 Abbou, J.; Demaille, C.; Druet, M.; Moiroux, J. Fabrication of Submicrometer-Sized Gold Electrodes of Controlled Geometry for Scanning Electrochemical-Atomic Force Microscopy. *Anal. Chem.* **2002**, *74*, 6355–6363.
21 Krapf, D.; Wu, M. Y.; Smeets, R. M. M.; Zandbergen, H. W.; Dekker, C.; Lemay, S. G. Fabrication and Characterization of Nanopore-Based Electrodes with Radii Down to 2 nm. *Nano Lett.* **2006**, *6*, 105–109.
22 Sun, P.; Mirkin, M. V. Kinetics of Electron-Transfer Reactions at Nanoelectrodes. *Anal. Chem.* **2006**, *78*, 6526–6534.
23 Sun, P.; Mirkin, M. V. Scanning Electrochemical Microscopy with Slightly Recessed Nanotips. *Anal. Chem.* **2007**, *79*, 5809–5816.
24 Zhang, B.; Galusha, J.; Shiozawa, P. G.; Wang, G.; Bergren, A. J.; Jones, R. M.; White, R. J.; Ervin, E. N.; Cauley, C. C.; White, H. S. Bench-Top Method for Fabricating Glass-Sealed Nanodisk Electrodes, Glass Nanopore Electrodes, and Glass Nanopore Membranes of Controlled Size. *Anal. Chem.* **2007**, *79*, 4778–4787.
25 Kim, Y. T.; Scarnulis, D. M.; Ewing, A. G. Carbon-Ring Electrodes with 1-μm Tip Diameter. *Anal. Chem.* **1986**, *58*, 1782–1786.
26 Strein, T. G.; Ewing, A. G. Characterization of Submicron-Sized Carbon Electrodes Insulated with a Phenol-Allylphenol Copolymer. *Anal. Chem.* **1992**, *64*, 1368–1373.
27 Strein, T. G.; Ewing, A. G. Characterization of Small Noble Metal Microelectrodes by Voltammetry and Energy-Dispersive X-Ray Analysis. *Anal. Chem.* **1993**, *65*, 1203–1209.
28 Meyerhoff, J. B.; Ewing, M. A.; Ewing, A. G. Ultrasmall Enzyme Electrodes with Response Time Less than 100 ms. *Electroanalysis* **1999**, *11*, 308–312.
29 Campbell, J. K.; Sun, L.; Crooks, R. M. Electrochemistry Using Single Carbon Nanotubes. *J. Am. Chem. Soc.* **1999**, *121*, 3779–3780.
30 Heller, I.; Kong, J.; Heering, H. A.; Williams, K. A.; Lemay, S. G.; Dekker, C. Individual Single-Walled Carbon Nanotubes as Nanoelectrodes for Electrochemistry. *Nano Lett.* **2005**, *5*, 137–142.
31 Burt, D. P.; Wilson, N. R.; Weaver, J. M. R.; Dobson, P. S.; Macpherson, J. V. Nanowire Probes for High Resolution Combined Scanning Electrochemical Microscopy - Atomic Force Microscopy. *Nano Lett.* **2005**, *5*, 639–643.
32 Obataya, I.; Nakamura, C.; Han, S. W.; Nakamura, N.; Miyake, J. Nanoscale Operation of a Living Cell Using an Atomic Force Microscope with a Nanoneedle. *Nano Lett.* **2005**, *5*, 27–30.
33 Kouklin, N. A.; Kim, W. E.; Lazareck, A. D.; Xu, J. M. Carbon Nanotube Probes for Single-Cell Experimentation and Assays. *Appl. Phys. Lett.* **2005**, *87*, 173901.
34 Freedman, J. R.; Mattia, D.; Korneva, G.; Gogotsi, Y.; Friedman, G.; Fontecchio, A. K. Magnetically Assembled Carbon Nanotube Tipped Pipettes. *Appl. Phys. Lett.* **2007**, *90*, 103108.
35 Chen, X.; Kis, A.; Zettl, A.; Bertozzi, C. R. A Cell Nanoinjector Based on Carbon Nanotubes. *Proc. Natl. Acad. Sci. U.S.A.* **2007**, *104*, 8218–8222.
36 Kim, W.; Ng, J. K.; Kunitake, M. E.; Conklin, B. R.; Yang, P. Interfacing Silicon Nanowires with Mammalian Cells. *J. Am. Chem. Soc.* **2007**, *129*, 7228–7229.
37 Yum, K.; Yu, M.-F. Surface-Mediated Liquid Transport through Molecularly Thin Liquid Films on Nanotubes. *Phys. Rev. Lett.* **2005**, *95*, 186102.
38 Zevenbergen, M. A. G.; Krapf, D.; Zuiddam, M. R.; Lemay, S. G. Mesoscopic Concentration Fluctuations in a Fluidic Nanocavity Detected by Redox Cycling. *Nano Lett.* **2007**, *7*, 384–388.
39 Tang, C.; Bando, Y.; Sato, T.; Kurashima, K. A Novel Precursor for Synthesis of Pure Boron Nitride Nanotubes. *Chem. Commun.* **2002**, *12*, 1290–1291.
40 Suryavanshi, A. P.; Yu, M.-F.; Wen, J.; Tang, C.; Bando, Y. Elastic Modulus and Resonance Behavior of Boron Nitride Nanotubes. *Appl. Phys. Lett.* **2004**, *84*, 2527–2529.
41 Yum, K.; Yu, M. F. Measurement of Wetting Properties of Individual Boron Nitride Nanotubes with the Wilhelmy Method Using a Nanotube-Based Force Sensor. *Nano Lett.* **2006**, *6*, 329–333.
42 Yum, K.; Wang, Z.; Suryavanshi, A. P.; Yu, M.-F. Experimental Measurement and Model Analysis of Damping Effect in Nanoscale Mechanical Beam Resonators in Air. *J. Appl. Phys.* **2004**, *96*, 3933–3938.
43 Finklea, H. O.; Snider, D. A.; Fedyk, J. Passivation of Pinholes in Octadecanethiol Monolayers on Gold Electrodes by Electrochemical Polymerization of Phenol. *Langmuir* **1990**, *6*, 371–376.
44 Chen, X.; Matsumoto, N.; Hu, Y.; Wilson, G. S. Electrochemically Mediated Electrodeposition/Electropolymerization to Yield a Glucose Microbiosensor with Improved Characteristics. *Anal. Chem.* **2002**, *74*, 368–372.
45 Wilson, N. R.; Macpherson, J. V. Single-Walled Carbon Nanotubes as Templates for Nanowire Conducting Probes. *Nano Lett.* **2003**, *3*, 1365–1369.
46 Suryavanshi, A. P.; Yu, M.-F. Electrochemical Fountain Pen Nanofabrication of Vertically Grown Platinum Nanowires. *Nanotechnology* **2007**, *18*, 105305.
47 Oldham, K. B. Steady State Voltammetry. In *Microelectrodes: Theory and Applications*; Montenegro, M. I., Queiros, M. A., Daschbach, J. L., Eds.; Kluwer Academic Publishers: Boston, 1991; pp 35–50.
48 Zoski, C. G. Steady-State Voltammetry at Microelectrodes. In *Modern Techniques in Electroanalysis*; Vanysek, P., Ed.; John Wiley & Sons: New York, 1996; pp 241–312.
49 Shoup, D.; Szabo, A. Influence of Insulation Geometry on the Current at Microdisk Electrodes. *J. Electroanal. Chem.* **1984**, *160*, 27–31.
50 Spaine, T. W.; Baur, J. E. A Positionable Microcell for Electrochemistry and Scanning Electrochemical Microscopy in Subnanoliter Volumes. *Anal. Chem.* **2001**, *73*, 930–938.

51 Ito, T.; Audi, A. A.; Dible, G. P. Electrochemical Characterization of Recessed Nanodisk-Array Electrodes Prepared from Track-Etched Membranes. *Anal. Chem.* **2006**, *78*, 7048–7053.

52 Birkin, P. R.; Silva-Martinez, S. Determination of Heterogeneous Electron Transfer Kinetics in the Presence of Ultrasound at Microelectrodes Employing Sampled Voltammetry. *Anal. Chem.* **1997**, *69*, 2055–2062.

53 Chen, S.; Kucernak, A. The Voltammetric Response of Nanometer-Sized Carbon Electrodes. *J. Phys. Chem. B* **2002**, *106*, 9396–9404.

54 Watkins, J. J.; White, H. S. The Role of the Electrical Double Layer and Ion Pairing on the Electrochemical Oxidation of Hexachloroiridate(III) at Pt Electrodes of Nanometer Dimensions. *Langmuir* **2004**, *20*, 5474–5483.

55 Krapf, D.; Quinn, B. M.; Wu, M. Y.; Zandbergen, H. W.; Dekker, C.; Lemay, S. G. Experimental Observation of Nonlinear Ionic Transport at the Nanometer Scale. *Nano Lett.* **2006**, *6*, 2531–2535.

56 Bard, A. J.; Faulkner, L. R. *Electrochemical Methods, Fundamentals and Applications*; John Wiley & Sons: New York, 2001.

57 The nanoelectrode was calibrated beforehand in a hemispherical microdroplet (~30 μm in radius) with the same nanowire reference electrode, where the solution concentration of the microdroplet was essentially constant during the measurement and the hysteresis between the forward and backward scans was not observed. The estimated apparent diameter of the nanoelectrode was ~50 nm.

58 Early studies with a microelectrode having a diameter of 7.5 μm also showed this deviation (*e.g.*, the current deficit) in both voltammetric and amperometric responses in picoliter-volume environments (75 pL in volume), as compared to in nanoliter volumes (4 nL) or bulk solutions (ref 5).

59 A linear form, $C(t) = C_i(1 + 0.0015t)$, also provides essentially the same voltammograms as in Figure 4c.

60 Vetter, K. J. *Electrochemical Kinetics, Theoretical and Experimental Aspects*; Academic Press: New York, 1967.